

Performance Analysis of Underwater Quantum Key Distribution Protocols: BB84, SARG04, and BBM92

Nour Rizk , Angélique Drémeau , and Arnaud Coatanhay 

Abstract

Underwater quantum key distribution (UQKD) ensures unconditional communication security based on the fundamental principles of quantum mechanics. This study examines the performance of the BB84, SARG04, and the entanglement-based BBM92 protocols under the impact of both system optical parameters and the physical effects of the underwater channel. The main performance criteria considered are the quantum bit error rate (QBER) and the quantum correlation between the communicating parties as functions of the propagation distance in three types of non-turbulent seawater: clear, coastal, and turbid. For the BBM92 protocol, the quantum channel is modeled using Kraus operators, which characterize the combined effects of attenuation and depolarization on maximally-entangled photons, allowing the derivation of our analytical expression of the QBER, based on the correlation losses between measurements. Monte Carlo simulation results validate the analytical expression of the QBER for all the studied protocols, under various water types, atmospheric conditions, and system parameters. The results determine the conditions under which QKD protocols achieve optimal performance for secure and efficient underwater quantum communications.

Index Terms

Quantum key distribution (QKD), underwater quantum communication, quantum entanglement, BB84 protocol, SARG04 protocol, BBM92 protocol, Kraus operators.

N. Rizk, A. Drémeau and A. Coatanhay are with Lab-STICC, UMR CNRS 6285, ENSTA, IP Paris, 29806 Brest, France.

I. INTRODUCTION

Underwater communications, whether between drones, submarines, underwater sensor networks, or various types of underwater vehicles, are often used to transmit highly sensitive informations. Ensuring the protection and confidentiality of this data is therefore a major challenge, especially in military applications. In this context, underwater optical wireless communication (UOWC) is particularly effective, offering both high bandwidth and an higher level of security compared to traditional acoustic communication [1]–[3]. However, since seawater is a dense scattering medium subject to multiple disturbances, propagation distance emerges as the primary limiting factor for optical signals range [4].

Critical security communications therefore rely on the exchange of private encryption keys. The main challenge, in this case, is to ensure that these keys are not intercepted or compromised by any third party. To address this issue, quantum cryptography, and particularly quantum key distribution (QKD), provides unconditional security based on the fundamental laws of quantum mechanics, such as the uncertainty principle and the no-cloning theorem [5], [6]. QKD allows two legitimate users, Alice and Bob, to establish a shared secret key over a quantum channel, where any interception attempt by an eavesdropper (Eve) can be detected. Since its first experimental demonstration in 1989 with a distance of 32 cm channels [7], great progress has been achieved in QKD over both free-space and optical fiber [8]–[10]. Early experiments covered only a few tens of centimeters, but later implementations achieved transmission distance through optical fibers exceeding 100 km, and eventually extended to satellite-based free-space links [11]. In these configurations, distances vary from about 500 km to several tens of thousands of kilometers, depending on the satellite orbit and the total attenuation typically below 60 dB [12]–[15]. Adapting this approach to the underwater environment opens new perspectives, where confidentiality requirements are increasingly critical, giving rise to underwater quantum key distribution (UQKD) [16], [17]. However, underwater optical conditions impose severe constraints on transmission distance, depolarization making it necessary to evaluate various QKD protocols. The performance of QKD protocols is described in terms of the quantum bit error rate (QBER), which measures errors in the transmitted quantum states and serves as an indicator of

both channel quality and potential eavesdropping. The first QKD protocol, BB84, was introduced by Bennett and Brassard in 1984 [18]. It is based on single-photon emission in four polarization states belonging to two orthonormal bases. It offers a low QBER and long transmission distances for an error threshold of 11% [19], but these results remain theoretical [20]. The first experimental demonstration of free-space underwater QKD was performed in 2017 over 3.3 m [16], followed by a successful implementation of the BB84 protocol in 2019 over 2.37 m [17]. Recently, research has explored BB84 under the effects of turbulence, temperature, and salinity, as well as in different water conditions [21], [22]. Although BB84 remains one of the most fundamental and widely implemented QKD protocols, it presents certain security limitations in experimental realizations. Imperfections in photon sources and detectors can expose the system to various attacks, such as photon number splitting (PNS) and detector side-channel attacks, thereby compromising the confidentiality of the generated key [23]. For this reason, many improved QKD protocols have been proposed to achieve higher security performance compared to BB84 [24]. For instance, SARG04 protocol is developed as a variant of BB84 to improve overall robustness and security [25]. Unlike BB84, where the key is encoded directly in the polarization basis, SARG04 encodes it using pairs of quantum states, which enhances protection against multi-photon vulnerabilities. However, SARG04 exhibits a higher QBER and a shorter maximum secure transmission distance (threshold of 14.9%) than BB84 [26]. Both protocols rely on the discrete-variable prepare-and-measure framework but differ in how Alice and Bob decide whether to keep or discard the received bits.

For an even higher level of security, a QKD protocol involving entanglement (entanglement-based QKD, EBQKD) between a pair of photons can be considered. For instance, the BBM92 protocol [27] is a well-known example. It is more sophisticated and harder to analyze than BB84 and SARG04, but it also provides stronger security, especially in environments where the communication channels are affected by strong attenuation and high noise, which modifies the quantum state polarization and superposition. In addition to traditional physical phenomena such as channel attenuation, the study requires modeling the decoherence induced on the photon pair by seawater.

Unlike protocols based on prepared states, a central source generates pairs of entangled photons

and sends one photon to Alice and the other to Bob. This configuration is useful for maritime architectures, where the source is positioned at a controlled depth underwater, while the receivers are placed on underwater drones or sensors. When two photons are entangled, any attempt by an eavesdropper to intercept or measure them changes their quantum correlation, which increases the QBER and limiting the achievable secure distance. This allows the legitimate users to detect an attack more easily, making the protocol more secure. However, it should be noted that this protocol significantly limits the communication range. As part of this study, one of the points we will seek to clarify is this reduction in distance.

Initially, the underwater link is modeled as an attenuating medium influenced by irradiance fluctuations and photonic noise. This simplified model provides preliminary performance estimations and enables the evaluation of the BB84 and SARG04 protocols. The obtained results are used to validate our simulation framework and to ensure consistency with existing literature. Motivated by the need for more comprehensive studies that account for realistic environmental effects, we extend our analysis to include additional quantum noise sources in order to achieve more accurate and secure underwater quantum communication systems. In practice, underwater channels not only cause attenuation but also induce photon depolarization and degrade entanglement. Well describing these phenomena is essential for evaluating the performance of UQKD protocols. Using this model, we analyze the BBM92 protocol using Kraus operators, under realistic underwater conditions.

The remainder of this article is organized as follows. Section II describes the system model and provides a detailed description of the protocols. The impact of the underwater channel on quantum transmission is analyzed in Section III. Section IV presents the analysis of quantum gain and QBER. The evolution of entangled states using Kraus operators in an underwater quantum channel is detailed in Section V. Section VI discusses the obtained results. Finally, the conclusions are presented in Section VII.

II. SYSTEM MODEL

In the standard EBQKD protocol, a source generates pairs of polarization-entangled photons that share correlated quantum information between two parties, Alice and Bob. One photon is

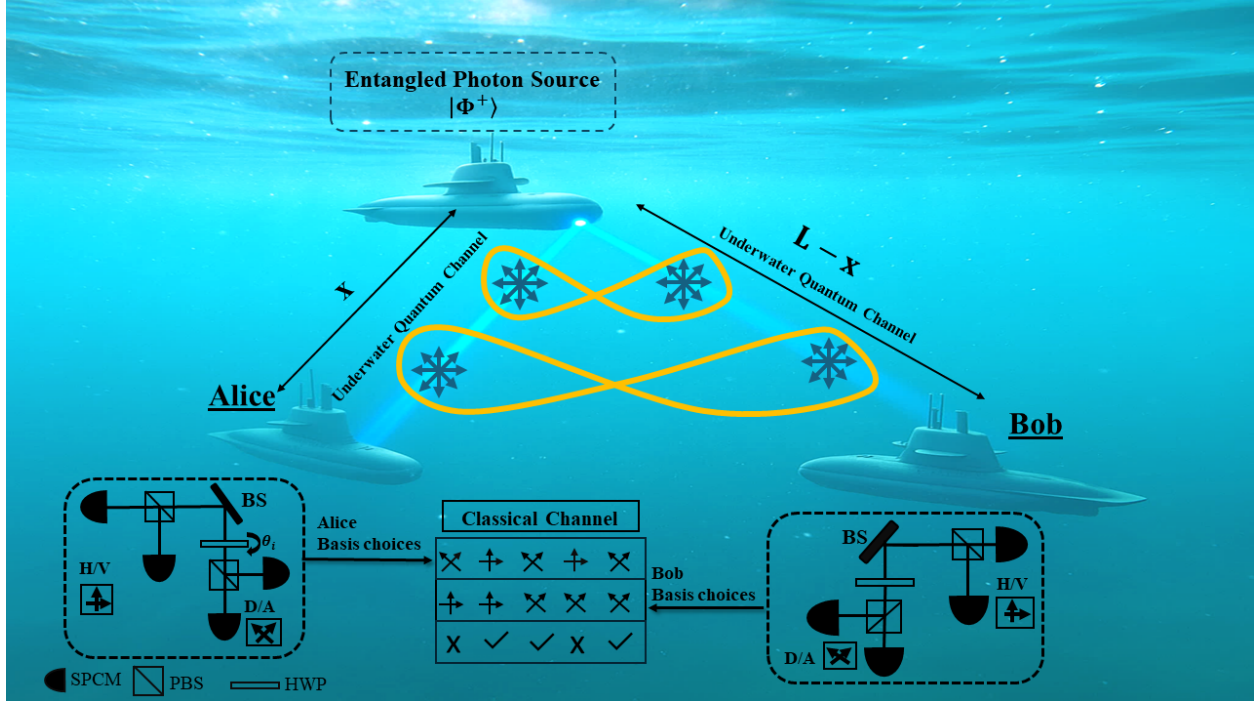


Fig. 1. Schematic diagram of BBM92 QKD protocol, where the HWP orientation θ_i sets the angles of the basis states.

transmitted to Alice, located at a distance x , and the other to Bob at $L - x$, through a non-turbulent underwater quantum channels, as illustrated in Fig. 1. When the source is located at Alice (i.e., $x = 0$), EBQKD is equivalent to the prepare-and-measure configuration used by BB84 and SARG04 protocols [18], [25]. To extract information, Alice and Bob randomly select a fraction of the received photons and perform polarization measurements in two orthonormal bases chosen at random, corresponding to four states (qubits) used to encode the classical bits 0 and 1: the rectilinear basis $H/V = \{|H\rangle, |V\rangle\}$ and the diagonal basis $D/A = \{|+\rangle, |-\rangle\}$. In the underwater environment, optical transmission is subject to physical phenomena such as attenuation, scattering, and the presence of suspended particles, which may induce photon losses or alter their polarization states. These effects reduce measurement precision and degrade entanglement fidelity, thereby impacting the overall performance of the protocol. After the measurements, Alice and Bob publicly announce their basis choices through a classical channel and retain only the results obtained from identical bases, which are then used to establish a secure secret key.

By changing the position of the source, the model can represent different QKD scenarios. When the source is placed in the middle (symmetrically) or closer to one user (asymmetrically), the measured correlations and the classical post-processing steps change accordingly. Our approach provides one framework to study and compare different QKD protocols.

A. BB84 protocol

The BB84 protocol, introduced by Bennett and Brassard in 1984 [18], relies on the transmission of photons prepared in two orthonormal bases, H/V and D/A . This configuration corresponds to the case where the source is located at Alice (i.e., $x = 0$), so that Alice prepares the quantum states and sends them directly to Bob. After the transmission and measurement phases, Alice and Bob publicly announce their basis choices over an authenticated classical channel, without revealing the bit values. They retain only the bits corresponding to identical bases, while the others are discarded. This step is referred to as the sifting process. To verify the integrity of the channel and detect possible eavesdropping, Alice and Bob reveal a random subset of the sifted bits and compare them, allowing the estimation of the QBER, defined as

$$\text{QBER}_{\text{BB84}} = \frac{\text{Number of erroneous sifted bits}}{\text{Total number of sifted bits}}. \quad (1)$$

Several studies in the literature have focused on the BB84 protocol because it achieves high performance under ideal conditions. However, even if BB84 performs efficiently, it remains less secure against certain attacks and eavesdropping attempts. It is considered secure only when the QBER stays below the analytical limit of 11% [19]. Beyond this value, it becomes difficult to separate errors caused by channel noise from those introduced by an eavesdropper (Eve). For this reason, more secure protocols have been proposed to improve protection against such attacks [28].

B. SARG04 protocol

SARG04 protocol, proposed by Scarani et al. in 2004 [25], was designed to enhance the security of QKD against PNS attacks, which exploit multiphoton emissions from weak coherent sources. As in BB84, the source is located at Alice ($x = 0$), who prepares the po-

larization states. The key difference lies in the sifting process: instead of directly revealing the measurement basis, Alice publicly announces a set of two non-orthogonal states chosen from $\{|H\rangle, |+\rangle\}$, $\{|H\rangle, |-\rangle\}$, $\{|V\rangle, |+\rangle\}$, $\{|V\rangle, |-\rangle\}$. Bob then compares his measurement outcome with the announced set. If his result is orthogonal to one of the two states, he can conclude that the photon corresponds to the other state, the bit is therefore conclusive. Otherwise, if his result is compatible with both states, it is inconclusive and discarded. The QBER is defined over the conclusive bits as

$$\text{QBER}_{\text{SARG04}} = \frac{\text{Number of erroneous conclusive bits}}{\text{Total number of conclusive bits}}. \quad (2)$$

The protocol remains secure as long as the QBER remains below 14.9% [29]. This threshold, which is higher than that of BB84, reflects better resistance to PNS attacks, although the conclusive bit rate is lower.

C. *BBM92 protocol*

The BBM92 protocol, proposed by Bennett, Brassard, and Mermin in 1992, is a variant of the BB84 protocol based on quantum entanglement EBQKD [27]. Unlike BB84 and SARG04, where Alice locally prepares the quantum states to be sent to Bob, BBM92 relies on a central source that generates entangled photon pairs and distributes one photon to Alice and the other to Bob (see Fig. 1). This configuration enhances security, since the key is established through quantum correlations rather than directly transmitted states, making it more resistant to certain eavesdropping attacks and channel disruptions. The photons are prepared in a Bell state belonging to the four-dimensional Hilbert space defined by the polarization states $\{|HH\rangle, |HV\rangle, |VH\rangle, |VV\rangle\}$, which maximizes the correlations between the two photons. In our study, we exclusively consider the state:

$$|\Phi^+\rangle = \frac{1}{\sqrt{2}}(|HH\rangle + |VV\rangle). \quad (3)$$

When both users perform their measurements in the same basis, their results are perfectly correlated. After a sufficiently large number of measurements in the H/V and D/A bases, Alice and Bob exchange, through an authenticated classical channel, the information regarding

their chosen bases. Only the results obtained with identical bases are retained, ensuring reliable correlations. Finally, a subset of these results is publicly revealed and compared in order to estimate the QBER, defined as:

$$\text{QBER}_{\text{BBM92}} = \frac{\text{Number of erroneous correlated bits}}{\text{Total number of correlated bits}}. \quad (4)$$

The BBM92 protocol theoretically achieves a QBER performance comparable to BB84, but with increased sensitivity to polarization variations. Both protocols share the same QBER threshold of 11% [30], above which secure key distribution cannot be maintained.

III. IMPACT OF THE UNDERWATER CHANNEL ON QUANTUM TRANSMISSION

In an underwater environment, quantum transmission is subject to physical constraints related to the optical properties of water. Unlike free-space or atmospheric communications, an underwater optical channel undergoes significant losses that compromise the fidelity of quantum states and limit the performance of QKD protocols. In our study, we consider the use of a collimated laser as the emission source, producing a narrow and stable beam. This configuration makes it possible to neglect geometric losses usually induced by beam divergence. The overall transmission efficiencies of the reception systems Alice and Bob can therefore be modeled as [31]

$$\eta_A = \eta_{\text{Alice}} \cdot A(x, \lambda), \quad (5)$$

$$\eta_B = \eta_{\text{Bob}} \cdot A(L - x, \lambda), \quad (6)$$

where η_{Alice} and η_{Bob} denote the detection efficiencies (including the quantum efficiency of the detectors), and $A(L, \lambda)$ is the underwater attenuation coefficient as a function of the distance L and the wavelength λ (see subsection III-A).

Three main phenomena influence the quality of transmission: attenuation, ambient irradiance, and photonic noise associated with the detectors. These effects have a direct impact on the performance of QKD protocols, particularly on the QBER, and consequently on the overall security of the transmission.

A. Underwater attenuation

In an underwater channel, the attenuation of the optical signal is mainly caused by two physical phenomena: absorption, resulting from the interaction of photons with water molecules that convert their energy into heat or chemical reactions, and scattering, corresponding to the deviation of photons from their initial trajectory due to suspended particles in the medium. These effects are characterized by the absorption coefficient $a(\lambda)$ and the scattering coefficient $b(\lambda)$, both depending on the wavelength λ , and vary depending on the type of water (clear, coastal, or turbid) [32]. In this study, attenuation is modeled using a modified version of the Beer-Lambert law, adapted to the geometric configuration of the laser source [33]

$$A(L, \lambda) = \exp \left(- \alpha(\lambda) L \left(\frac{d_1}{\theta L} \right)^T \right), \quad (7)$$

where θ is the divergence angle of the emitted beam, d_1 the transmitter aperture diameter, T a correction factor depending on the water type (see Table I), and L the propagation distance. This linear model is well suited to probabilistic analyzes of photon transmission in QKD, in contrast to classical telecommunication approaches, which preferentially consider logarithmic expressions.

B. Photonic noise sources

In addition to propagation losses, the performance of the QKD system is affected by photonic noise produced within the detection devices. This noise reduces the reliability of measurements and therefore affects the overall safety of the system. Two main sources of photonic noise are considered :

- Background optical noise (n_B), caused by residual ambient light in the underwater environment. These photons are randomly detected by the receiver and cannot be distinguished from real signal photons. Inside the reception module, optical components such as the beam splitter (BS) and polarizing beam splitters (PBS) distribute these photons randomly among the four avalanche photodiodes (APDs). A detector is composed of a PBS and two APDs. Assuming uniform distribution, each detector receives then on average half of this noise, i.e., $n_B/2$.

- “Dark counts” (n_D), generated by the intrinsic operation of the detectors. Even in the absence of incoming photons, photodetectors can produce random electrical pulses, known as “dark current” I_{dc} , characterised by an average false click rate (in Hz) specific to each detector.

The average total noise affecting each detector can therefore be expressed as [22], [34]

$$n_N = n_D + \frac{n_B}{2}. \quad (8)$$

From this expression, the average number of noise photons detected across the system during a pulse of duration Δt , within a receiver gate time $\Delta t'$, can be estimated as [35]

$$y_0 = 4n_N = 4I_{dc} \Delta t + \frac{R S \Delta t' \lambda \Delta \lambda \Omega}{h_p c_{\text{light}}}, \quad (9)$$

where R represents the underwater irradiance (see subsection III-C), $S \triangleq \pi (d_2/2)^2$ is the area of the receiver aperture with d_2 the lens diameter, h_p Planck’s constant, c_{light} the speed of light, $\Delta \lambda$ the filter bandwidth and Ω is the solid angle of reception given by

$$\Omega \triangleq 2\pi \left(1 - \cos \left(\frac{\delta}{2} \right) \right), \quad (10)$$

with δ the field-of-view angle of the detector. This expression derives from spherical geometry, representing the solid angle subtended by a cone of half-angle of $\delta/2$. A higher value of δ corresponds to a higher value of Ω , which means that the receiver captures light over a larger spatial region.

It is important to note that, in this experimental context, the term y_0 is less than 1 and can be considered as the probability of a photon being present due to noise.

C. Underwater irradiance

Underwater irradiance, denoted $R(z, \lambda)$, quantifies the amount of ambient light present in the water. It comes mainly from sunlight or artificial light sources. This light is added to the background noise n_B in subsection (III-B). As depth z increases, irradiance decreases exponentially [32]

$$R(z, \lambda) = R_0(\lambda) e^{-K_\infty z}, \quad (11)$$

where $R_0(\lambda)$ is the irradiance at the surface level for wavelength λ and K_∞ is the diffuse attenuation coefficient governing the exponential decay with depth.

IV. PERFORMANCE METRIX FOR UQKD COMMUNICATION SYSTEM

This section presents the performance of the BB84, SARG04, and BBM92 protocols in terms of quantum gain and QBER, considering a non-turbulent underwater channel.

A. Quantum gain

Unlike idealized analytical models in which every pulse contains exactly one photon, experimental QKD transmitters use attenuated laser light. In quantum optics, these pulses are described as weak coherent states with random phase, the number of photons N per pulse following a Poisson distribution with mean μ . Accordingly, the probability that a given pulse contains i photons is

$$\mathbb{P}(N = i) = \frac{\mu^i}{i!} e^{-\mu}, \quad i \in \mathbb{N}. \quad (12)$$

Let A_i denote the event “the pulse contains exactly i photons”. Applying the law of total probability, the quantum gain Q_μ is defined as the sum, for all photon numbers i , of the product of the probability that Alice emits a state with i photons, as described in (12), and the conditional probability that this state with i photons (including photon noise) will result in a detection event on Bob’s side, say $Y_i \triangleq \mathbb{P}(\text{click} \mid A_i)$. Formally, it is expressed as [36]

$$\begin{aligned} Q_\mu &:= \mathbb{P}(\text{at least one detected click}), \\ &= \sum_{i=0}^{\infty} \mathbb{P}(\text{click} \mid A_i) \cdot \mathbb{P}(A_i) = \sum_{i=0}^{\infty} Y_i \cdot \frac{\mu^i}{i!} e^{-\mu}. \end{aligned} \quad (13)$$

Now, to further characterise the quantum gain achievable by the system, it is necessary to specify the form of Y_i as a function of the physical parameters of the system. If the pulse contains at least one photon ($i \geq 1$), the probability that none will be detected after transmission through a channel with efficiency η_X is $(1 - \eta_X)^i$, where $X \in \{A, B\}$, A and B representing Alice and Bob, respectively. Thus, the probability that at least one photon is detected is $1 - (1 - \eta_X)^i$. In this context, two events may lead to a detector click:

- a true detection, corresponding to the reception of at least one photon from the signal, with a probability $1 - (1 - \eta_X)^i$;
- a false detection, independent of the signal, caused by background noise or intrinsic effects of the detector, and thus modelled by the average probability y_0 per pulse (see (9)).

1) *Quantum gain for BB84*: For the BB84 protocol, the total probability of detecting a pulse containing i photons can be expressed as the sum of the two independent events presented above. Since y_0 is very small, the case where true detection and false detection occur simultaneously can be neglected. For $i \geq 1$ and $\eta_A = 1$, the total detection probability can therefore be approximated as

$$\begin{aligned}
 Y_i^{(\text{BB84})} &= \mathbb{P}(\text{click} \mid A_i), \\
 &= \mathbb{P}(\text{true detection} \mid A_i) + \mathbb{P}(\text{false detection} \mid A_i), \\
 &\approx [1 - (1 - \eta_B)^i] + y_0.
 \end{aligned} \tag{14}$$

Note that when no photon is emitted ($i = 0$), this probability reduces to $Y_0^{(\text{BB84})} = y_0$. By inserting this expression into (13), and taking into account the Poissonian statistics of weak coherent pulses, one obtains:

$$Q_{\mu, \text{BB84}} = y_0 + 1 - e^{-\eta_B \mu}. \tag{15}$$

This compact relation highlights the two independent mechanisms leading to a detector click. The proof is provided in Appendix-A.

2) *Quantum gain for SARG04*: In the SARG04 protocol [37], a key bit is only generated when a detector click can be interpreted as a conclusive event. Bob must then deduce with certainty the transmitted bit from his measurement basis, the result obtained, and the set of non-orthogonal states announced by Alice. Consequently, only a fraction of the detection events directly affects the overall probability of winning. Applying the total probability law to the number of photons

$N \sim \text{Poisson}(\mu)$, we obtain

$$\begin{aligned} Q_{\mu, \text{SARG04}} &= \sum_{i=0}^{\infty} \mathbb{P}(\text{conclusive click} \mid A_i) \cdot \mathbb{P}(A_i), \\ &= \sum_{i=0}^{\infty} Y_i^{(\text{SARG04})} \cdot \frac{\mu^i}{i!} e^{-\mu}, \end{aligned} \quad (16)$$

where $Y_i^{(\text{SARG04})}$ denotes the probability of obtaining a conclusive click given that the pulse contains exactly i photons.

Case $i = 0$. When the pulse is empty, any detection originates from noise with probability y_0 . Considering the eight possible configurations (four sets of Alice's states and two sets of Bob's measurement bases), two lead to a correct conclusive result, two to a conclusive error, and four are inconclusive. The probability of obtaining a correct conclusive click is therefore $1/4$, yielding

$$Y_0^{(\text{SARG04})} = \frac{1}{4} y_0, \quad Q_{\mu, \text{SARG04}}^{(0)} = \frac{1}{4} y_0 e^{-\eta_B \mu}. \quad (17)$$

Case $i \geq 1$. For a pulse containing at least one photon, the probability of a true detection is $1 - (1 - \eta_B)^i$. Among these detections, $1/4$ corresponds to conclusive correct clicks and $e_{\text{det}}/2$ corresponds to conclusive errors, where e_{det} is the probability of an error due to the sensors, i.e. taking into account imperfections in the measuring device such as decoherence or instrumental noise. The total probability that a click is conclusive (whether correct or erroneous) is therefore $\frac{1}{4} + \frac{e_{\text{det}}}{2}$. We then obtain

$$Y_i^{(\text{SARG04})} = [1 - (1 - \eta_B)^i] \left(\frac{1}{4} + \frac{e_{\text{det}}}{2} \right), \quad (18)$$

and

$$\begin{aligned} Q_{\mu, \text{SARG04}}^{(1+)} &= \sum_{i=1}^{\infty} Y_i^{(\text{SARG04})} \cdot \frac{\mu^i}{i!} e^{-\mu}, \\ &= \left(\frac{1}{4} + \frac{e_{\text{det}}}{2} \right) \cdot \sum_{i=1}^{\infty} [1 - (1 - \eta_B)^i] \cdot \frac{\mu^i}{i!} e^{-\mu}, \\ &= \left(\frac{1}{4} + \frac{e_{\text{det}}}{2} \right) (1 - e^{-\eta_B \mu}). \end{aligned} \quad (19)$$

By combining both expressions (17) and (19), the overall quantum gain for the SARG04 protocol

is expressed as

$$Q_{\mu, \text{SARG04}} = \underbrace{\frac{1}{4} y_0 e^{-\eta_B \mu}}_{\text{noise}} + \underbrace{\left(\frac{1}{4} + \frac{e_{\text{det}}}{2} \right) (1 - e^{-\eta_B \mu})}_{\text{true signal}}. \quad (20)$$

3) *Quantum gain for BBM92*: Unlike the BB84 and SARG04 protocols, where calculating quantum gain requires adding up all possible pulse sizes weighted by the Poisson distribution, the BBM92 protocol follows a different logic. In this protocol, a bit is only retained when an entangled pair leads to simultaneous detections at Alice's and Bob's detectors in the same time window, i.e. a coincidence. The event is therefore no longer 'one click is observed', but rather 'two clicks are observed simultaneously', and the gain is deduced directly from the probability of coincidence. For each user $X \in \{A, B\}$, two independent events are modelled. The first, denoted S_X , is the successful transmission of an entangled photon, which occurs with probability $(1 - e^{-\eta_X \mu})$, where μ is the average number of photons. The second, denoted N_X , corresponds to the replacement of the photon by a noise photon, with probability y_0 . The presence of a photon in X is therefore $C_X = S_X \cup N_X$, and a coincidence is defined as $(C_A \cap C_B)$. This event includes true coincidences $(S_A \cap S_B)$, double noise events $(N_A \cap N_B)$ and accidental coincidences $((S_A \cap N_B)$ and $(N_A \cap S_B))$. Assuming independence, the probability of coincidence writes

$$\begin{aligned} Q_{\mu, \text{BBM92}} &= \mathbb{P}_{\text{coinc}} = \mathbb{P}(C_A \cap C_B), \\ &= \mathbb{P}((S_A \cup N_A) \cap (S_B \cup N_B)), \\ &= \mathbb{P}(S_A \cap S_B) + \mathbb{P}(S_A \cap N_B) + \mathbb{P}(N_A \cap S_B) + \mathbb{P}(N_A \cap N_B), \\ &= (1 - e^{-\eta_A \mu}) (1 - e^{-\eta_B \mu}) + y_0 (1 - e^{-\eta_A \mu}) + y_0 (1 - e^{-\eta_B \mu}) + y_0^2, \\ &= \underbrace{\eta_A \eta_B}_{\mathbb{P}_{\text{true}}} + \underbrace{y_0 (\eta_A + \eta_B) + y_0^2}_{\mathbb{P}_{\text{false}}}, \end{aligned} \quad (21)$$

where we introduce \mathbb{P}_{true} as the probability of a true coincidence $(S_A \cap S_B)$, and $\mathbb{P}_{\text{false}}$ as the probability of counting accidental or noise-induced coincidences. For an attenuated laser, the approximation $1 - e^{-\eta_X \mu} \approx \eta_X \mu$ (first-order expansion) can be considered, since single-photon

events dominate and higher-order contributions can be neglected.

B. QBER

The QBER is a fundamental measure of the quality of the correlations exploited in QKD protocols. In a more general formulation, encompassing the different definitions expressed in Section II, the QBER can be mathematically stated as:

$$\text{QBER} = \frac{E_\mu}{Q_\mu}, \quad (22)$$

where Q_μ denotes the overall quantum gain, as discussed in the previous subsection, and E_μ represents the contribution of erroneous events to this gain.

A high QBER value may indicate either excessive noise in the system or an active eavesdropping attempt. In the following, we derive the analytical expressions of the QBER for each of the considered protocols (BB84, SARG04, and BBM92), based on the previously established expressions of the quantum gain [37].

1) *QBER for BB84*: In the BB84 protocol, errors mainly originate from two sources. The first corresponds to errors in detecting signal photons due to sensor imperfections, characterised by an error probability e_{det} . The second source is related to false clicks, i.e., detection events triggered by noise photons of the photodetectors. Unlike signal photons, these clicks occur randomly and therefore carry no information about the prepared polarization state. Since each measurement basis (H/V or D/A) involves two detectors, a spurious click has a probability of 50% of producing a correct bit and 50% of introducing an error. Consequently, the associated error probability is $e_0 = \frac{1}{2}$.

The total errors in the BB84 protocol can therefore be expressed as

$$E_{\mu,\text{BB84}} = \frac{1}{2}y_0 + e_{\text{det}}(1 - e^{-\eta_B\mu}). \quad (23)$$

The QBER is obtained by taking the ratio between the number of errors given in (23) and

the total gain defined in (15)

$$\text{QBER}_{\text{BB84}} = \frac{e_0 y_0 + e_{\text{det}} (1 - e^{-\eta_B \mu})}{Q_{\mu, \text{BB84}}}. \quad (24)$$

2) *QBER for SARG04*: In the SARG04 protocol, only conclusive detection events are used for key generation. This specificity modifies both the expression of the gain and the error structure compared to the BB84 protocol. The QBER is therefore defined as the ratio between the total number of errors from conclusive detections and the overall gain of the protocol. Two types of errors are considered. The first originates from false clicks: as in BB84, they occur randomly, but only a fraction of them is retained as conclusive; protocol analysis shows that one quarter of these clicks are both retained and erroneous. The second source is related to the detection of signal photons: only conclusive detections are taken into account, and half of the errors associated with these events are effectively preserved. The total number of errors is obtained by combining these two terms. Using (20), the QBER for the SARG04 protocol is then expressed as

$$\text{QBER}_{\text{SARG04}} = \frac{\frac{1}{4} y_0 e^{-\eta_B \mu} + \frac{e_{\text{det}}}{2} (1 - e^{-\eta_B \mu})}{Q_{\mu, \text{SARG04}}}. \quad (25)$$

3) *QBER for BBM92*: In the BBM92 protocol, the QBER is evaluated from the coincidence detections between Alice and Bob [20]. Its expression accounts for two types of errors. The first one corresponds to measurement errors occurring on the detected entangled photon pairs. The second arises from false coincidences, which introduce a random error with a probability of 50%. By combining these effects, the QBER of BBM92 can be derived as a function of the probability of obtaining a true coincidence \mathbb{P}_{true} and that of a false coincidence $\mathbb{P}_{\text{false}}$

$$\text{QBER}_{\text{BBM92}} = \frac{e_{\text{det}} \cdot \mathbb{P}_{\text{true}} + \frac{1}{2} \cdot \mathbb{P}_{\text{false}}}{Q_{\mu, \text{BBM92}}}. \quad (26)$$

The position of the entangled-photon source directly influences the QBER of BBM92 protocol. An asymmetric configuration, where the source is located near one user, increases the

transmission distance for the other photon, leading to higher losses and a greater probability of false coincidences, thereby raising the $\text{QBER}_{\text{BBM92}}$. Moreover, when the source is positioned at $x = 0$ (i.e. at Alice), (26) reduces to the expression of the BB84 protocol (24), demonstrating the consistency between the two models and confirming that BBM92 is a symmetric generalization of BB84 protocol. The $\text{QBER}_{\text{BBM92}}$ attains its minimum for a symmetric placement of the source, i.e., at a distance halfway between Alice and Bob. A complete derivation is presented in Appendix B.

V. EVOLUTION OF THE ENTANGLED STATE USING KRAUS OPERATORS IN AN UNDERWATER QUANTUM CHANNEL

This section extends the classical submarine channel model to a quantum framework in order to describe how environmental parameters influence the evolution of an entangled state. The underwater medium is modeled as a noisy open quantum system, where photon interactions with the environment induce decoherence and irreversible dynamics.

In this study, Alice and Bob share a pair of qubits prepared in a maximally entangled Bell state, represented by the density matrix $\rho_{AB}^{\text{in}} = |\Phi^+\rangle\langle\Phi^+|$, expressed in the canonical basis $|00\rangle, |01\rangle, |10\rangle, |11\rangle$, which forms an orthonormal basis of the bipartite Hilbert space $\mathcal{H}_{AB} = \mathcal{H}_A \otimes \mathcal{H}_B$. In an ideal isolated system, this state evolves as $\rho_{AB}^{\text{in}} \rightarrow U\rho_{AB}^{\text{in}}U^\dagger$ with U a unitary operator, preserving both information and entanglement [38]. In contrast, when transmitted through an underwater channel, the evolution becomes non-unitary and is described by a completely positive and trace-preserving (CPTP) map represented by a set of Kraus operators $\{K_j\}$. The number of Kraus operators ‘ n ’ depends on the dimension ‘ d ’ of the Hilbert space of the system, such that $n \leq d^2$. For a qubit, as a superposition of two states $d = 2$, we need $n = 4$ Kraus operators [38], [39].

Each Kraus operator K_j represents an interaction between the system and its environment, collectively describing how the underwater channel modifies the quantum state and degrades the entanglement shared between Alice and Bob. If the channel acts only on the photon B transmitted to one user “Bob”, while the other photon A “Alice” remains unaffected, the evolution of the

bipartite system is given by

$$\rho_{AB}^{\text{out}} = \mathcal{E}(\rho_{AB}^{\text{in}}) = \sum_{j=0}^{n-1} K_j \rho_{AB}^{\text{in}} K_j^\dagger, \quad (27)$$

where the Kraus operators satisfy the unitarity condition $\sum_{j=0}^{n-1} K_j^\dagger K_j = \mathbb{I}_2$.

In our model, the evolution of the entangled state is modeled by two successive quantum channels: an amplitude-damping channel $\mathcal{E}_{\text{damp}}$ followed by a depolarizing channel \mathcal{E}_{dep} , described in Sections V-A and V-B. This sequence reflects the physical reality of underwater propagation and is essential because quantum operations are non-commutative ($\mathcal{E}_{\text{damp}} \circ \mathcal{E}_{\text{dep}} \neq \mathcal{E}_{\text{dep}} \circ \mathcal{E}_{\text{damp}}$).

A. Amplitude Damping Channel

In underwater quantum communication, the amplitude attenuation channel is used to model the energy loss experienced by photons as they pass through a medium. This loss mainly comes from absorption and scattering caused by water molecules and suspended particles, which reduce the probability that the photon stays in its excited quantum state. Therefore, the amplitude-damping mechanism provides a description of photon attenuation and the gradual loss of quantum coherence in such environments [40]. Mathematically, its action on a qubit is expressed using a set of Kraus operators $\{K_0, K_1, K_2, K_3\}$, which depend on two parameters:

- the parameter $p = 1 - e^{-A(L,\lambda)} \in [0, 1]$, which represents the attenuation rate in the underwater channel,
- the thermal parameter $\xi \in [0, \frac{1}{2}]$, which expresses the average quantity of thermal photons in the channel.

The amplitude damping channel is then described by the following four Kraus operators

$$K_0 = I_A \otimes \sqrt{1-\xi} \begin{pmatrix} 1 & 0 \\ 0 & \sqrt{1-p} \end{pmatrix}, \quad K_2 = I_A \otimes \sqrt{\xi} \begin{pmatrix} 0 & 0 \\ \sqrt{p} & 0 \end{pmatrix},$$

$$K_1 = I_A \otimes \sqrt{1-\xi} \begin{pmatrix} 0 & \sqrt{p} \\ 0 & 0 \end{pmatrix}, \quad K_3 = I_A \otimes \sqrt{\xi} \begin{pmatrix} \sqrt{1-p} & 0 \\ 0 & 1 \end{pmatrix},$$

where \otimes stands for the Kronecker product.

In the BBM92 protocol, each photon is affected by an independent amplitude damping channel: photon A by $\mathcal{E}_{\text{damp}}^A$ and photon B by $\mathcal{E}_{\text{damp}}^B$. The overall evolution of the bipartite state is then described by

$$\begin{aligned}\rho_{AB}^{\text{out-damp}} &= (\mathcal{E}_{\text{damp}}^A \otimes \mathcal{E}_{\text{damp}}^B) \cdot \rho_{AB}^{\text{in}}, \\ &= \sum_{i,j} (K_i^A \otimes K_j^B) \rho_{AB}^{\text{in}} (K_i^A \otimes K_j^B)^\dagger.\end{aligned}\quad (28)$$

To obtain the global evolution, the operators K_{ij} are constructed by taking the Kronecker product of the local operators acting on Alice's and Bob's subsystems, $K_{ij} = K_i^A \otimes K_j^B$ where $i, j \in \{0, 1, 2, 3\}$. However, in an underwater channel with temperatures between $T = 15^\circ\text{C}$ and 26°C , and for an optical wavelength of $\lambda = 530\text{ nm}$, the mean number of thermal photons ξ is given by the Bose–Einstein distribution

$$\xi = \frac{1}{\exp\left(\frac{h\nu}{kT}\right) - 1}, \quad \nu = \frac{c}{\lambda}, \quad (29)$$

where h is Planck's constant, k is Boltzmann's constant and c is the speed of light in vacuum. For these values, one obtains $\xi \simeq 0$. Thus, thermal noise can be neglected, and the Kraus operators associated with thermal excitation $\{K_2, K_3\}$ have a negligible effect on the evolution of the system. The channel is therefore modelled in a simplified form, retaining only two operators, K_0 and K_1 , that is $\{K_0^A, K_1^A\}$ for Alice's channel and $\{K_0^B, K_1^B\}$ for Bob's channel. The corresponding parameters are defined as $p_A = 1 - e^{-A(x,\lambda)}$ and $p_B = 1 - e^{-A(L-x,\lambda)}$, with transmission amplitudes given by $t_A = \sqrt{1 - p_A}$ and $t_B = \sqrt{1 - p_B}$. The action of each $\{K_{ij}\}$ for $i, j \in \{0, 1\}$ on the initial state $|\Phi^+\rangle$ yields the intermediate states

$$|\psi_{ij}\rangle = K_{ij} |\Phi^+\rangle. \quad (30)$$

These four states describe all possible evolutions of the entangled state through both amplitude damping channels. By combining them (see Appendix-C for the details of the derivation), the

final state of the system can be reconstructed as

$$\begin{aligned}\rho_{AB}^{\text{out-damp}} &= \sum_{i,j=0}^1 |\psi_{ij}\rangle \langle \psi_{ij}|, \\ &= \begin{pmatrix} a_0 & 0 & 0 & f_0 \\ 0 & b_0 & 0 & 0 \\ 0 & 0 & c_0 & 0 \\ f_0 & 0 & 0 & d_0 \end{pmatrix},\end{aligned}\quad (31)$$

where

$$\begin{aligned}a_0 &= \frac{1}{2}(1 + p_A p_B), & b_0 &= \frac{1}{2}p_A T_B, & c_0 &= \frac{1}{2}p_B T_A, \\ d_0 &= \frac{1}{2}T_A T_B, & f_0 &= \frac{1}{2}t_A t_B, & T_A &= t_A^2, & T_B &= t_B^2.\end{aligned}$$

B. Depolarizing Channel

The depolarizing quantum channel \mathcal{E}_{dep} represents a type of noise that makes a qubit lose part of its quantum information. It does not flip the state directly, it replaces the pure state with a completely mixed state with a certain probability, thereby reducing both quantum coherence and superposition fidelity. To model the effect of a unilateral depolarizing channel, i.e., when Bob's photon passes through the channel, the initial density state ρ_{AB}^{in} is transformed as follows

$$\mathcal{E}_{\text{dep}}(\rho_{AB}^{\text{in}}) = (1 - q)\rho_{AB}^{\text{in}} + \frac{q}{3} \sum_{i=x,y,z} (I_A \otimes \sigma_i) \rho_{AB}^{\text{in}} (I_A \otimes \sigma_i), \quad (32)$$

where the parameter $q = 1 - e^{-\gamma_{\text{dep}}L} \in [0, 1]$ represents the depolarization probability, γ_{dep} is the linear depolarization coefficient and the operators σ_i ($i = x, y, z$) are the Pauli matrices, defined as

$$\sigma_x = \begin{pmatrix} 0 & 1 \\ 1 & 0 \end{pmatrix}, \quad \sigma_y = \begin{pmatrix} 0 & -i \\ i & 0 \end{pmatrix}, \quad \sigma_z = \begin{pmatrix} 1 & 0 \\ 0 & -1 \end{pmatrix}. \quad (33)$$

In the absence of direct measurements of γ_{dep} at 530 nm in underwater channels, we rely on the experimental results at 810 nm [16], together with an estimation based on the absorption spectra of different water types, which suggests a reduction factor of about 10^{-2} [41]. The details and

derivations are given in Appendix-D. The values of γ_{dep} are summarized in Table I.

We adopt a more operational representation of (32) to describe the evolution of the system under the depolarising channel, using four Kraus operators $\{L_i(q)\}$ defined as:

$$\begin{aligned} L_0(q) &= \sqrt{1-q} I, & L_1(q) &= \sqrt{\frac{q}{3}} \sigma_x, \\ L_2(q) &= \sqrt{\frac{q}{3}} \sigma_y, & L_3(q) &= \sqrt{\frac{q}{3}} \sigma_z, \end{aligned} \quad (34)$$

where I denotes the identity matrix and $\sigma_x, \sigma_y, \sigma_z$ are the Pauli matrices. In the context of the BBM92 protocol, where each of the two photons (Alice's and Bob's) passes through an independent depolarizing channel, the global Kraus operators $\{L_{ij}\}$ acting on the bipartite system are obtained as the tensor product of the local Kraus operators applied to each subsystem:

$$L_{ij} = L_i(q_A) \otimes L_j(q_B), \quad i, j \in \{0, 1, 2, 3\} \quad (35)$$

where $q_A = 1 - e^{-\gamma_{\text{dep}}x}$ and $q_B = 1 - e^{-\gamma_{\text{dep}}(L-x)}$ are the depolarization probabilities in Alice's and Bob's channels, respectively.

The final state of the system, after passing through the two channels, is obtained by applying the set of 16 Kraus operators to the density matrix $\rho_{AB}^{\text{out-damp}}$ in (31)

$$\begin{aligned} \rho_{AB}^{\text{out-dep}} &= \sum_{i,j=0}^3 L_{ij} \rho_{AB}^{\text{out-damp}} L_{ij}^\dagger, \\ &= \begin{pmatrix} a_1 & 0 & 0 & k_1 \\ 0 & b_1 & 0 & 0 \\ 0 & 0 & c_1 & 0 \\ k_1 & 0 & 0 & d_1 \end{pmatrix}. \end{aligned} \quad (36)$$

where

$$\left\{ \begin{array}{l} a_1 = n_A n_B a_0 + n_A s_B b_0 + s_A n_B c_0 + s_A s_B d_0, \\ b_1 = n_A s_B a_0 + n_A n_B b_0 + s_A s_B c_0 + s_A n_B d_0, \\ c_1 = s_A n_B a_0 + s_A s_B b_0 + n_A n_B c_0 + n_A s_B d_0, \\ d_1 = s_A s_B a_0 + s_A n_B b_0 + n_A s_B c_0 + n_A n_B d_0, \\ k_1 = f_A f_B f_0, \\ n_{A,B} = 1 - \frac{4}{3} q_{A,B}, \quad s_{A,B} = \frac{2}{3} q_{A,B}, \quad f_{A,B} = 1 - \frac{4}{3} q_{A,B}. \end{array} \right.$$

C. QBER analysis for BBM92 using Kraus operators

To accurately evaluate the performance of the BBM92 protocol in an underwater quantum channel, it is necessary to establish a relationship between the quantum correlations degraded by the Kraus operators and the quantum bit error rate (QBER), defined as

$$\text{QBER}_{\text{BBM92}} = \frac{e_{\text{sig}} \cdot \mathbb{P}_{\text{true}} + \frac{1}{2} \mathbb{P}_{\text{false}}}{\mathbb{P}_{\text{true}} + \mathbb{P}_{\text{false}}}. \quad (37)$$

The signal error event associated with true coincidence detections, denoted as E_{sig} and characterized by the probability e_{sig} , arises from two distinct mechanisms. The first corresponds to a channel-induced quantum state change, described by the Kraus operators and occurring with probability $\mathbb{P}_{\text{Kraus}}$, while the detector functions correctly with probability $(1 - e_{\text{det}})$. The second mechanism occurs when the channel preserves the quantum state $(1 - \mathbb{P}_{\text{Kraus}})$, but the detector introduces an error with probability e_{det} . From these two cases, one obtains

$$e_{\text{sig}} = e_{\text{det}} + (1 - 2e_{\text{det}}) \cdot \mathbb{P}_{\text{Kraus}}. \quad (38)$$

The quantum correlation $\langle \sigma_x \otimes \sigma_x \rangle = \text{Tr}(\rho_{AB}^{\text{out-dep}}(\sigma_x \otimes \sigma_x))$ quantifies the statistical dependence between the measurement outcomes of the two qubits. This correlation reflects how much of the shared quantum information is preserved or degraded during transmission, and it is directly linked to the Kraus probability

$$\mathbb{P}_{\text{Kraus}} = \frac{1 - \langle \sigma_x \otimes \sigma_x \rangle}{2}. \quad (39)$$

The correlation $\langle \sigma_z \otimes \sigma_z \rangle$ remains almost unaffected by the channel, indicating that this observable is weakly sensitive to the dominant error mechanisms. In contrast, the reduction of $\langle \sigma_x \otimes \sigma_x \rangle$ reflects the decoherence of the system and governs the evolution of the QBER.

VI. RESULTS AND DISCUSSION

We investigate the QBER performance of the BB84, SARG04, and BBM92 protocols, as well as the quantum correlation of the BBM92 protocol, under various non-turbulent underwater channel conditions. Both environmental parameters, including the water type (clear, coastal, and turbid) according to Mobley's classification [32], and five distinct atmospheric conditions are considered [42] :

- 1) Scenario 1: clear atmosphere, full moon near the zenith, i.e., $R_0(\lambda) = 10^{-3} \text{ W/m}^2$;
- 2) Scenario 2: heavy overcast, sun near the horizon, i.e., $R_0(\lambda) = 10 \text{ W/m}^2$;
- 3) Scenario 3: hazy atmosphere, sun near the horizon, i.e., $R_0(\lambda) = 50 \text{ W/m}^2$;
- 4) Scenario 4: heavy overcast, sun at the zenith, i.e., $R_0(\lambda) = 125 \text{ W/m}^2$;
- 5) Scenario 5: clear atmosphere, sun at the zenith, i.e., $R_0(\lambda) = 500 \text{ W/m}^2$.

The analysis also takes into account system parameters such as the transmitter and receiver pupil diameters. The analytical expressions of the QBER, presented in sections IV-B and V-C, are compared with Monte Carlo simulation results described in section II. For the simulations, 10000 photon packets, each containing 1000 photons, are emitted by a source located at a distance x from Alice and $L - x$ from Bob. The theoretical and numerical results presented below are obtained using a subset of parameters summarized in Table I, which are taken from [21], [22].

Fig. 2 illustrates the QBER performance of the BB84 and SARG04 protocols as a function of transmission distance in a non-turbulent underwater channel under nighttime conditions with a full moon, corresponding to Scenario 1. The study considers different transmitter and receiver aperture diameters ($d_1 = d_2 = 5, 10, 20, \text{ and } 30 \text{ cm}$) and three water types: clear, coastal, and turbid. The analytical and Monte Carlo simulation results match perfectly, confirming the validity of the models used. It is observed that the QBER of the SARG04 protocol is approximately twice as high as that of BB84 at all distances [43], for different pupil diameters and atmospheric

Table I: System and channel parameters

Parameter	Definition	Value
λ	Wavelength [22]	530 nm
θ	Divergence angle of the beam	6°
δ	Detector aperture [22]	180°
$\Delta\lambda$	Filter spectral width [21]	0.2 nm
Δt	Bit period [21]	40 ns
$\Delta t'$	Receiver gate time [21]	200 ps
d_1	Transmitter pupil diameter	30 cm
d_2	Receiver pupil diameter	30 cm
$\eta_{\text{Alice, Bob}}$	Quantum efficiency of Geiger-mode APDs [22]	0.5
μ	Mean photon number per pulse	1
K_∞	Asymptotic diffuse attenuation coefficient [22]	0.08 m ⁻¹
I_{dc}	Dark current count rate [22]	60 Hz
z	Depth [21]	80 m
e_{det}	Detection error rate [22]	3.3%
α	Extinction coefficient [32]	
	Clear water	0.151 m ⁻¹
	Coastal water	0.339 m ⁻¹
T	Correction coefficient [22]	
	$d_1 = d_2 = 5$ cm	0.13
	$d_1 = d_2 = 10$ cm	0.16
	$d_1 = d_2 = 20$ cm	0.21
γ_{dep}	Depolarization coefficient	
	Clear water	$2.4 \times 10^{-6} \text{m}^{-1}$
	Coastal water	$3.7 \times 10^{-6} \text{m}^{-1}$
	Turbid water	$7.5 \times 10^{-6} \text{m}^{-1}$

conditions, indicating higher stability for SARG04. In clear water, the maximum transmission distance increases with the pupil diameter. For BB84, it reaches 125.84 m, 134.64 m, 153.34 m, and 179.05 m for pupil diameters of 5 cm, 10 cm, 20 cm, and 30 cm, respectively. For SARG04, the corresponding values are 116.50 m, 124.28 m, 141.10 m, and 163.43 m, as shown in Fig. 2(a). This improvement is attributed to the larger collection of signal photons when the background noise is minimal, resulting in a higher signal-to-noise ratio (SNR) and a longer achievable transmission distance. In Fig. 2(b), corresponding to coastal water, a similar behavior is observed, although with shorter transmission distances due to stronger scattering and absorption. For BB84,

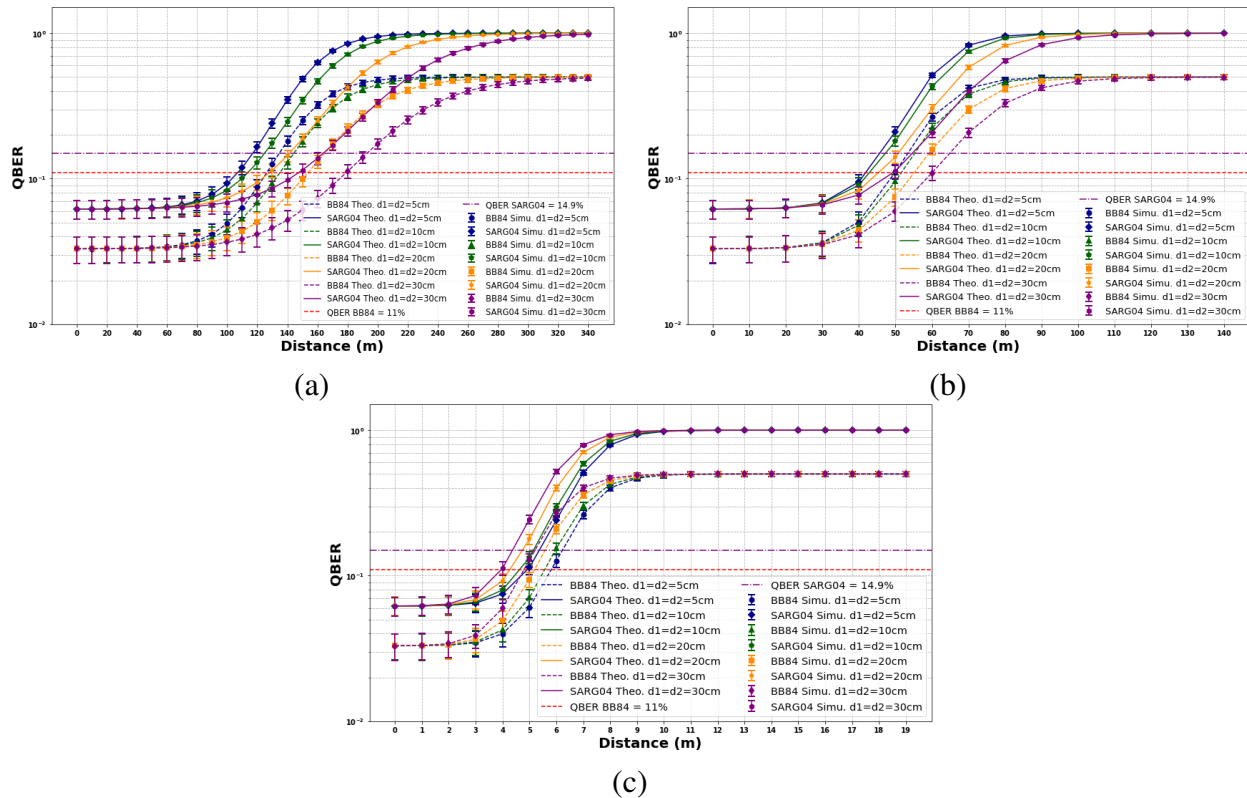


Fig. 2. $QBER_{BB84}$ and $QBER_{SARG04}$ vs. distance for Scenario 1, with $R_0(\lambda) = 10^{-3} \text{ W/m}^2$, and different pupil diameters in (a) clear water, (b) coastal water, and (c) turbid water.

the transmission range increases from 49.78 m to 60.05 m, while for SARG04, it varies from 44.64 m to 53.81 m at $d_1 = 5$ cm and 30 cm, respectively. In Fig. 2(c), an opposite behavior is observed, where the transmission distance decreases with increasing pupil diameter. The distance decreases from 5.75 m to 4.73 m for BB84 and from 5.28 m to 4.28 m for SARG04, respectively. In highly scattering channels, a wider pupil diameter captures more noise photons, leading to an increase in photonic noise, which reduces the SNR and consequently degrades the transmission quality.

Fig. 3 shows the same experimental configuration under daytime conditions corresponding to Scenario 5. In this situation, the ambient irradiance becomes the dominant limiting factor and the beneficial effect of a larger pupil diameter observed at night disappears. In clear water, the maximum transmission range for BB84 drops from 54.63 m to 7.86 m, while for SARG04, it decreases from 46.43 m to 4.39 m at $d_1 = 5$ cm and 30 cm, respectively. In Fig. 3(b), a more significant performance reduction is observed compared to Fig. 2(b), the range decreases

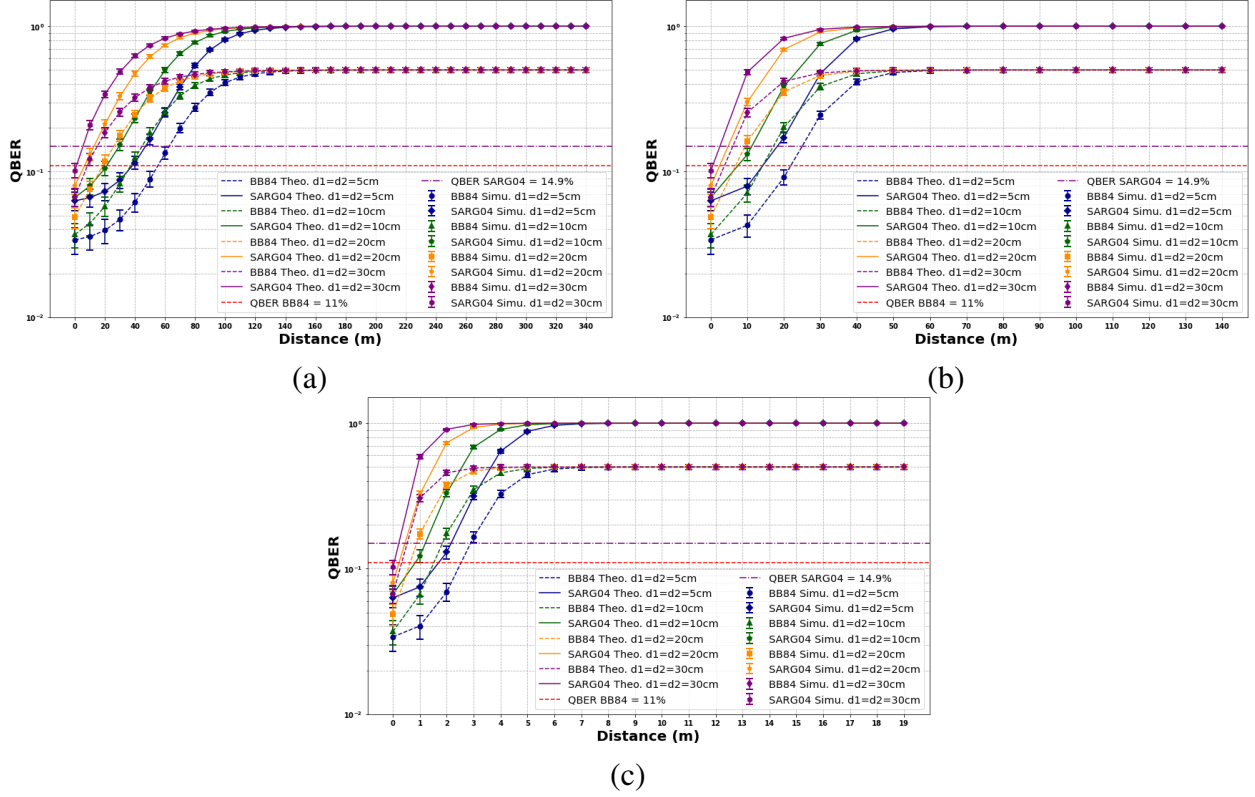


Fig. 3. $QBER_{BB84}$ and $QBER_{SARG04}$ vs. distance for Scenario 5, with $R_0(\lambda) = 500 \text{ W/m}^2$, and different pupil diameters in (a) clear water, (b) coastal water, and (c) turbid water.

from 49.78 m to 21.20 m and from 60.05 m to 2.28 m, for BB84 at night and during the day, respectively. For SARG04, it drops to 17.50 m and 1.23 m, respectively. In turbid water, the transmission range becomes extremely short. For BB84, the distance decreases from 2.43 m to 0.18 m, and for SARG04, from 2.10 m to 0.10 m at $d_1 = 5 \text{ cm}$ and 30 cm, respectively, as shown in Fig. 3(c). Compared to the nighttime case in Fig. 2(c), this represents a reduction of over 60% in maximum range, resulting from the combined impact of strong turbidity and high irradiance. Under these conditions, background noise dominates the received signal and drastically reduces the secure transmission range.

These results demonstrate that the water type, underwater irradiance, and pupil diameter have a significant impact on the performance of underwater QKD systems. As turbidity increases, signal attenuation becomes stronger, resulting in a marked reduction in the maximum transmission distance. Furthermore, the maximum achievable distance during daytime is significantly lower than that at nighttime due to the increase in background noise. This reduction in range is

more pronounced for SARG04, which is more affected by underwater channel-induced errors. Consequently, the quantum gain is lower, and the QBER is generally higher for the SARG04 protocol compared to BB84.

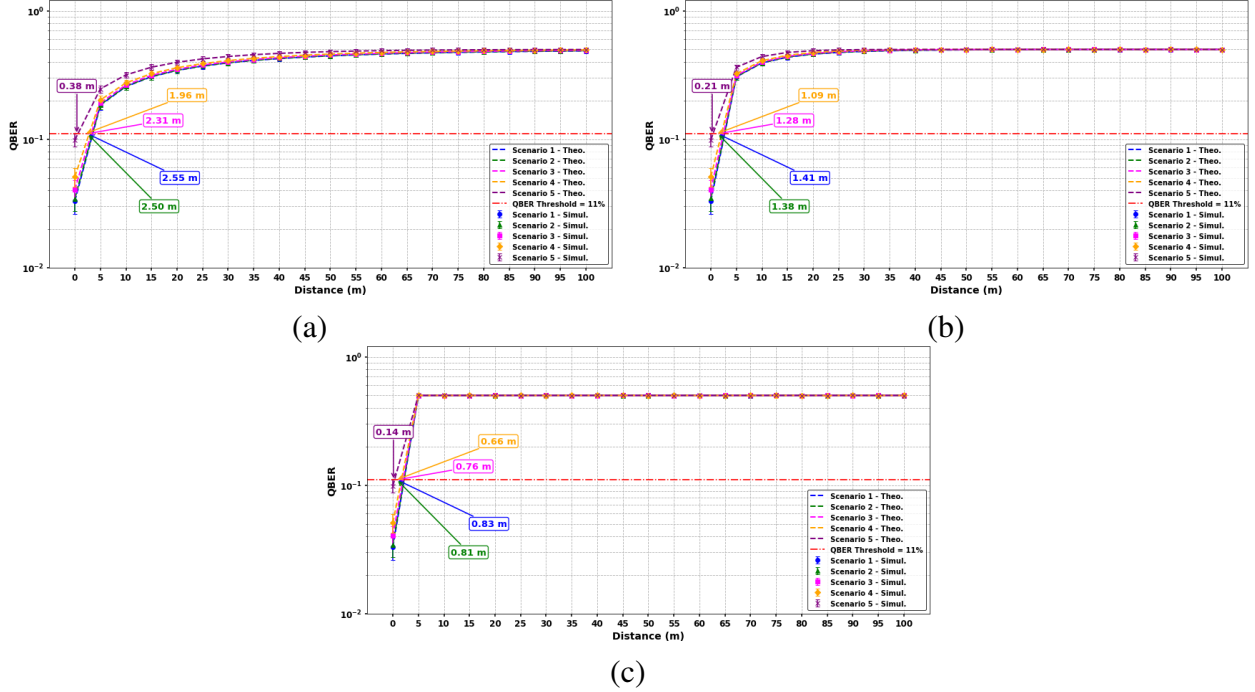


Fig. 4. $\text{QBER}_{\text{BBM92}}$ vs. distance for different scenarios, with $x = L/2$, in (a) clear water, (b) coastal water, and (c) turbid water.

Fig. 4 illustrates the QBER of the BBM92 protocol described by (37) as a function of transmission distance for the five light scenarios considered, in three types of water (clear, coastal, and turbid) and $d_1 = 30$ cm, when the source of entangled pairs is placed in the middle of the optical link ($x = L/2$). In this study, the underwater quantum channel is modeled using Kraus operators, which successively describe the effects of optical attenuation and depolarization (loss of polarization coherence). We observe that the theoretical and Monte Carlo simulation curves coincide almost perfectly, confirming the validity of the proposed model. In Fig. 4(a), the QBER increases gradually with distance and remains below the 11% threshold up to about 2.55 m in Scenario 1, while this threshold is reached around 0.38 m in Scenario 5, under strong illumination. As water turbidity increases, the maximum transmission distance decreases: for coastal water, it drops from about 1.41 m to 0.21 m, and for turbid water, from 0.83 m to 0.14 m, for Scenarios

1 and 5, as shown in Fig. 4(b) and Fig. 4(c), respectively. These results reflect the influence of attenuation and depolarization: as the scattering level increases, the coherence of the entangled state degrades, leading to a higher QBER.

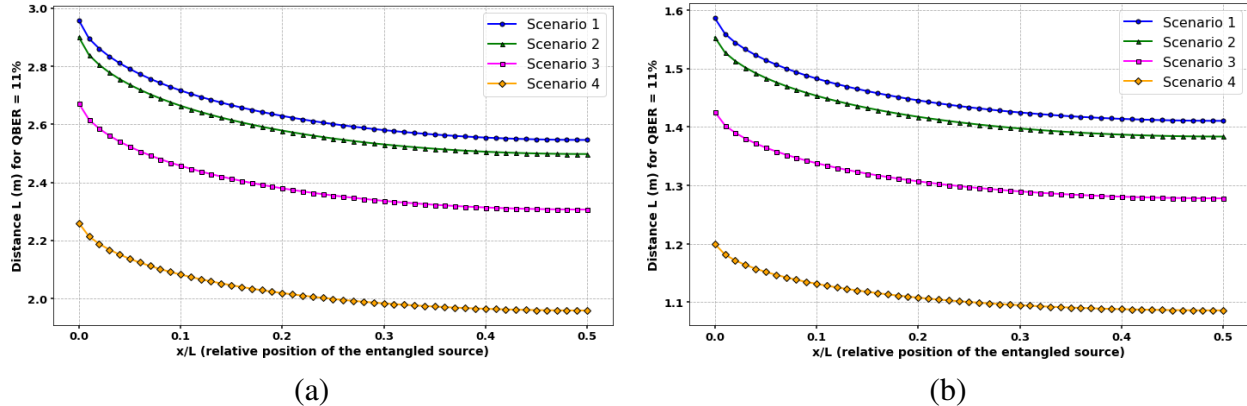


Fig. 5. Maximum secure transmission distance where the $\text{QBER}_{\text{BBM92}} = 11\%$ vs. relative position of the entangled source x/L in (a) clear water and (b) coastal water.

Fig. 5 shows the variation of the maximum secure transmission distance L , corresponding to the distance where the QBER of the BBM92 protocol reaches 11%, as a function of the relative position of the entangled source x/L .

In clear water, L gradually decreases as the source moves from Alice's side ($x = 0$) toward the center of the underwater channels ($x = 0.5L$). The secure distance decreases from approximately 2.96 m to 2.55 m in Scenario 1, and from 2.26 m to 1.96 m in Scenario 4, with Scenarios 2 and 3 following the same exponential trend, as shown in Fig. 5(a). Increasing underwater irradiance enhances photonic noise, which raises the QBER and thus limits the achievable secure range.

Fig. 5(b) corresponds to coastal water, which is more absorbing and scattering than clear water, the same decreasing behavior of L with x/L is observed, but with smaller values. In Scenario 1, the distance decreases from about 1.59 m to 1.41 m, whereas in Scenario 4 it drops from 1.20 m to 1.09 m. This reduction results from the higher attenuation coefficient of coastal water compared with clear water.

In turbid water, the achievable secure transmission distance remains almost unchanged for all scenarios and source positions Fig. 4(c). This is due to the strong optical attenuation and rapid degradation of entanglement, which dominate the system performance and make the source

position have negligible effect on the secure range.

These results show that the source position strongly affects the BBM92 protocol performance when the underwater channel is modeled using Kraus operators. The symmetric configuration balances optical losses but is not optimal in a noisy channel, as identical depolarization acting on both photons weakens the measured entanglement correlation. When the source is placed closer to Alice ($x < 0.5L$), each photon propagates through its own damping and depolarization channel with different characteristics: the longer path to Bob leads to stronger photon scattering and depolarization, causing a reduction in the correlation of the entangled state. This channel asymmetry reduces the overall depolarization and enhances the fidelity of the shared entangled state.

This analysis differs from that obtained using the model without Kraus operators, described by (26). In that case, the best performance is achieved when the source is placed at the midpoint of the link ($x = L/2$). As the source moves closer to one user, the transmission distance decreases, eventually showing the same behavior as the BB84 protocol when the source is located at Alice's side ($x = 0$).

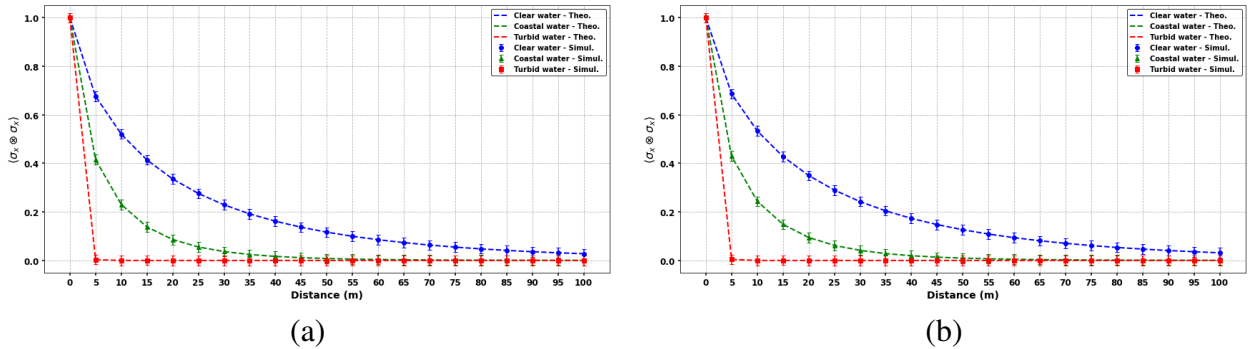


Fig. 6. Correlation $\langle \sigma_x \otimes \sigma_x \rangle$ vs. distance in different types of water (clear, coastal, and turbid) for (a) $x = L/2$, and (b) $x = 0.2L$.

Fig. 6 shows the evolution of the quantum correlation as a function of the transmission distance for the three types of water: clear, coastal, and turbid, when the entangled photon source is placed at the center of the optical link, i.e., $x = L/2$. Analytical and Monte Carlo simulation results are perfectly matching, confirming the validity of the model based on Kraus operators used. At short distances, the correlation is maximum for all water types, indicating that the entanglement is well

preserved. As the transmission distance increases, the correlation decreases rapidly due to the effects of amplitude damping channel and depolarizing channel. This decay is most pronounced in turbid water, where strong scattering and absorption cause the correlation to drop almost to zero after only a few meters. In coastal water, the correlation decreases more slowly but becomes negligible beyond approximately 60 m, while in clear water, a measurable correlation remains even up to 100 m. The same tendency can be observed in the QBER results: as the correlation decreases faster in more turbid water, the QBER increases more rapidly, limiting the maximum transmission distance. Therefore, placing the source closer to one user reduces the average depolarization effect on the system and results in a higher quantum correlation, especially in clear and coastal waters.

VII. CONCLUSION

In this article, we analyzed the performance of the BB84, SARG04, and BBM92 QKD protocols in non-turbulent underwater quantum channels. The study quantified the evolution of the QBER and quantum correlations under various environmental and system configurations. The results show that the transmission distance strongly depends on the pupil diameter, irradiance conditions, and water turbidity. In clear water under low irradiance, larger apertures enhance photon collection and extend the secure transmission distance. Conversely, in turbid water or under daylight conditions, an increased aperture size amplifies background noise and degrades performance. The SARG04 protocol exhibits a higher QBER than BB84 and a shorter maximum secure transmission distance under all considered conditions. For the BBM92 protocol, we derived an analytical expression for the QBER using Kraus operators. This approach describes the influence of attenuation and depolarization, which are two dominant factors affecting the preservation of entanglement in underwater photon transmission. For the BB84, SARG04 and BBM92 protocols, the analytical expressions of the QBER were successfully validated through Monte Carlo simulations, for different water types, irradiance scenarios and system parameters. Moreover, it is observed that the water turbidity and the ambient irradiance degrade the quantum correlation between entangled photons by enhancing depolarization and photonic noise, which increases the QBER and reduce the secure transmission distance. The analysis also highlights

the importance of the entangled source position: in asymmetric configurations, the quantum correlation between photons is better preserved, the entangled-state fidelity remains higher, and the QBER decreases, thereby allowing for a longer secure transmission distance.

APPENDIX A

QUANTUM GAIN FOR BB84

Using (13) and the Poissonian distribution of weak coherent pulses, we obtain:

$$\begin{aligned}
Q_{\mu, \text{BB84}} &= \sum_{i=0}^{\infty} Y_i^{(\text{BB84})} \cdot \frac{\mu^i}{i!} e^{-\mu}, \\
&= \sum_{i=1}^{\infty} [1 - (1 - \eta)^i + y_0] \cdot \frac{\mu^i}{i!} e^{-\mu} + y_0 \cdot e^{-\mu}, \\
&= y_0 \cdot \left(\sum_{i=1}^{\infty} \frac{\mu^i}{i!} e^{-\mu} + e^{-\mu} \right) + \sum_{i=1}^{\infty} [1 - (1 - \eta)^i] \cdot \frac{\mu^i}{i!} e^{-\mu}, \\
&= y_0 + \sum_{i=1}^{\infty} [1 - (1 - \eta)^i] \cdot \frac{\mu^i}{i!} e^{-\mu}, \\
&= y_0 + \sum_{i=1}^{\infty} \frac{\mu^i}{i!} e^{-\mu} - \sum_{i=1}^{\infty} (1 - \eta)^i \frac{\mu^i}{i!} e^{-\mu}, \\
&= y_0 + (e^{\mu} - 1)e^{-\mu} - (e^{(1-\eta)\mu} - 1)e^{-\mu}, \\
&= y_0 + 1 - e^{-\eta\mu}.
\end{aligned} \tag{A.1}$$

APPENDIX B

IMPACT OF THE SOURCE POSITION ON THE QBER_{BMM92}

The rate of false coincidence can be modeled as a function

$$f(x) = y_0 \eta_{\text{Alice}} A(x) + y_0 \eta_{\text{Bob}} A(L - x) + y_0^2, \tag{B.1}$$

and its derivative is given by

$$\begin{aligned}
f'(x) &= -y_0 \eta_{\text{Alice}} \alpha \left(\frac{d_1}{\theta} \right)^T (1 - T) x^{-T} e^{-\alpha x} \left(\frac{d_1}{\theta x} \right)^T \\
&\quad + y_0 \eta_{\text{Bob}} \alpha \left(\frac{d_1}{\theta} \right)^T (1 - T) (L - x)^{-T} e^{-\alpha(L-x)} \left(\frac{d_1}{\theta(L-x)} \right)^T.
\end{aligned} \tag{B.2}$$

By applying a straightforward optimization, one finds that the false coincidence rate is minimized when $f'(x) = 0$, then

$$\eta_{Alice} x^{-T} e^{-\alpha x (\frac{d_1}{\theta x})^T} = \eta_{Bob} (L - x)^{-T} e^{-\alpha (L-x) (\frac{d_1}{\theta(L-x)})^T}. \quad (\text{B.3})$$

When $\eta_{Alice} = \eta_{Bob}$, the condition (B.3) is satisfied for $x = L/2$, resulting in the minimization of $\text{QBER}_{\text{BBM92}}$.

APPENDIX C

MODELING OF AN UNDERWATER QUANTUM DAMPING CHANNEL

The operators $\{K_{ij}\}$ in (28) are

$$\begin{aligned} K_{00} &= \begin{pmatrix} 1 & 0 & 0 & 0 \\ 0 & t_B & 0 & 0 \\ 0 & 0 & t_A & 0 \\ 0 & 0 & 0 & t_A t_B \end{pmatrix}, & K_{01} &= \begin{pmatrix} 0 & \sqrt{p_B} & 0 & 0 \\ 0 & 0 & 0 & 0 \\ 0 & 0 & 0 & t_A \sqrt{p_B} \\ 0 & 0 & 0 & 0 \end{pmatrix}, \\ K_{10} &= \begin{pmatrix} 0 & 0 & \sqrt{p_A} & 0 \\ 0 & 0 & 0 & t_B \sqrt{p_A} \\ 0 & 0 & 0 & 0 \\ 0 & 0 & 0 & 0 \end{pmatrix}, & K_{11} &= \begin{pmatrix} 0 & 0 & 0 & \sqrt{p_A p_B} \\ 0 & 0 & 0 & 0 \\ 0 & 0 & 0 & 0 \\ 0 & 0 & 0 & 0 \end{pmatrix}. \end{aligned} \quad (\text{C.1})$$

The action of these operators on the initial state $|\Phi^+\rangle$ yields the vectors $|\psi_{ij}\rangle$ defined in (30), explicitly

$$\begin{aligned} |\psi_{00}\rangle &= \frac{1}{\sqrt{2}} \begin{pmatrix} 1 \\ 0 \\ 0 \\ t_A t_B \end{pmatrix}, & |\psi_{01}\rangle &= \frac{1}{\sqrt{2}} \begin{pmatrix} 0 \\ 0 \\ \sqrt{p_B} t_A \\ 0 \end{pmatrix}, \\ |\psi_{10}\rangle &= \frac{1}{\sqrt{2}} \begin{pmatrix} 0 \\ \sqrt{p_A} t_B \\ 0 \\ 0 \end{pmatrix}, & |\psi_{11}\rangle &= \frac{1}{\sqrt{2}} \begin{pmatrix} \sqrt{p_A p_B} \\ 0 \\ 0 \\ 0 \end{pmatrix}. \end{aligned} \quad (\text{C.2})$$

From these vectors, the projected density matrices are constructed

$$\begin{aligned}
\rho_{00} &= \frac{1}{2} \begin{pmatrix} 1 & 0 & 0 & t_A t_B \\ 0 & 0 & 0 & 0 \\ 0 & 0 & 0 & 0 \\ t_A t_B & 0 & 0 & (t_A t_B)^2 \end{pmatrix}, & \rho_{01} &= \frac{1}{2} \begin{pmatrix} 0 & 0 & 0 & 0 \\ 0 & 0 & 0 & 0 \\ 0 & 0 & p_B t_A^2 & 0 \\ 0 & 0 & 0 & 0 \end{pmatrix}, \\
\rho_{10} &= \frac{1}{2} \begin{pmatrix} 0 & 0 & 0 & 0 \\ 0 & p_A t_B^2 & 0 & 0 \\ 0 & 0 & 0 & 0 \\ 0 & 0 & 0 & 0 \end{pmatrix}, & \rho_{11} &= \frac{1}{2} \begin{pmatrix} p_A p_B & 0 & 0 & 0 \\ 0 & 0 & 0 & 0 \\ 0 & 0 & 0 & 0 \\ 0 & 0 & 0 & 0 \end{pmatrix}.
\end{aligned} \tag{C.3}$$

The final state is obtained as the sum of the four matrices

$$\begin{aligned}
\rho_{AB}^{\text{out-damp}} &= \rho_{00} + \rho_{01} + \rho_{10} + \rho_{11} \\
&= \frac{1}{2} \begin{pmatrix} 1 + p_A p_B & 0 & 0 & t_A t_B \\ 0 & p_A t_B^2 & 0 & 0 \\ 0 & 0 & p_B t_A^2 & 0 \\ t_A t_B & 0 & 0 & (t_A t_B)^2 \end{pmatrix}.
\end{aligned} \tag{C.4}$$

APPENDIX D

ESTIMATION OF THE DEPOLARIZATION COEFFICIENT

The approach proposed in [16], consists of comparing quantum correlation measured before and after transmission through a 3 m underwater channel. In an ideal Bell state, the observable $\langle \sigma_X \otimes \sigma_X \rangle$ takes its maximum value in the absence of noise, meaning that the information is perfectly conserved. Conversely, when one of the photons passes through a depolarizing channel, this correlation decreases. We then define the ratio

$$R = \frac{V_{\text{out}}}{V_{\text{in}}}, \tag{D.1}$$

where $V_{\text{in}} = \text{Tr}(\rho_{AB}^{\text{in}}(\sigma_X \otimes \sigma_X))$ and V_{out} represent the correlations before and after depolarization, respectively. To explicitly compute V_{out} , we apply the action of the depolarizing channel to

the correlation

$$\begin{aligned} V_{\text{out}} &= (1 - q)V_{\text{in}} + \frac{q}{3} \sum_{i=x,y,z} \text{Tr}[(I_A \otimes \sigma_i) \rho_{AB}^{\text{in}} (I_A \otimes \sigma_i) (\sigma_x \otimes \sigma_x)], \\ &= (1 - q)V_{\text{in}} + \frac{q}{3} \sum_{i=x,y,z} \text{Tr}[\rho_{AB}^{\text{in}} (\sigma_x \otimes (\sigma_i \sigma_x \sigma_i))], \end{aligned} \quad (\text{D.2})$$

where

$$\sigma_i \sigma_x \sigma_i = \begin{cases} \sigma_x & \text{si } i = x, \\ -\sigma_x & \text{si } i \neq x. \end{cases}$$

We deduce

$$q = \frac{3}{4}(1 - R). \quad (\text{D.3})$$

Using the experimental measurements, $V_{\text{in}} = 0.9528$, $V_{\text{out}} = 0.9499$, and $L = 3$ m, we obtain $q = 0.00225$ and $\gamma_{\text{dep}}(810 \text{ nm}) = -\frac{1}{L} \ln(1 - q) = 7.5 \times 10^{-4} \text{ m}^{-1}$.

ACKNOWLEDGMENTS

The authors would like to express their gratitude to the Brittany Region for its support and funding of this research.

REFERENCES

- [1] T. Theocharidis and E. Kavallieratou, “Underwater communication technologies: A review,” *Telecommunication Systems*, vol. 88, no. 2, p. 54, 2025, <http://doi.org/10.1007/s11235-025-01279-x>.
- [2] H. Kaushal and G. Kaddoum, “Underwater optical wireless communication,” *IEEE access*, vol. 4, pp. 1518–1547, 2016, <http://doi.org/10.1109/ACCESS.2016.2552538>.
- [3] M. O. Lanzagorta, *Underwater communications*. Morgan & Claypool Publishers, 2012, <http://doi.org/10.1007/978-3-031-01678-3>.
- [4] Y. Baykal, Y. Ata, and M. Gökçe, “Underwater turbulence, its effects on optical wireless communication and imaging: A review,” *Optics & Laser Technology*, vol. 156, p. 108624, 2022, <http://doi.org/10.1016/j.optlastec.2022.108624>.
- [5] P. Busch, T. Heinonen, and P. Lahti, “Heisenberg’s uncertainty principle,” *Physics reports*, vol. 452, no. 6, pp. 155–176, 2007, <http://doi.org/10.1016/j.physrep.2007.05.006>.
- [6] W. K. Wootters and W. H. Zurek, “A single quantum cannot be cloned,” *Nature*, vol. 299, no. 5886, pp. 802–803, 1982, <http://doi.org/10.1038/299802a0>.
- [7] C. H. Bennett, F. Bessette, G. Brassard, L. Salvail, and J. Smolin, “Experimental quantum cryptography,” *Journal of cryptology*, vol. 5, no. 1, pp. 3–28, 1992, <http://doi.org/10.1007/BF00191318>.

- [8] H. Takesue, E. Diamanti, C. Langrock, M. M. Fejer, and Y. Yamamoto, “10-GHz clock differential phase shift quantum key distribution experiment,” *Optics Express*, vol. 14, no. 20, pp. 9522–9530, 2006, <http://doi.org/10.1364/oe.14.009522>.
- [9] H. Takesue, S. Nam, Q. Zhang, R. Hadfield, T. Honjo, K. Tamaki, and Y. Yamamoto, “Quantum key distribution over a 40-dB channel loss using superconducting single-photon detectors,” *Nature photonics*, vol. 1, no. 6, pp. 343–348, 2007, <http://doi.org/10.1038/nphoton.2007.75>.
- [10] S. Wang, W. Chen, J. F. Guo, Z. Q. Yin, H. W. Li, Z. Zhou, G. C. Guo, and Z. F. Han, “2 GHz clock quantum key distribution over 260 km of standard telecom fiber,” *Optics Letters*, vol. 37, no. 6, pp. 1008–1010, 2012, <http://doi.org/10.1364/OL.37.001008>.
- [11] W. Buttler, R. Hughes, P. Kwiat, S. Lamoreaux, G. Luther, G. Morgan, J. Nordholt, C. Peterson, and C. Simmons, “Practical free-space quantum key distribution over 1 km,” *Physical review letters*, vol. 81, no. 15, p. 3283, 1998, <http://doi.org/10.1103/PhysRevLett.81.3283>.
- [12] V. Sharma, C. Shukla, S. Banerjee, and A. Pathak, “Controlled bidirectional remote state preparation in noisy environment: a generalized view,” *Quantum Information Processing*, vol. 14, no. 9, pp. 3441–3464, 2015, <http://doi.org/10.1007/s11128-015-1038-5>.
- [13] J. Sidhu, S. Joshi, M. Gündoğan, T. Brougham, D. Lowndes, L. Mazzarella, M. Krutzik, S. Mohapatra, D. Dequal, G. Vallone, and al., “Advances in space quantum communications,” *IET Quantum Communication*, vol. 2, no. 4, pp. 182–217, 2021, <http://doi.org/10.1049/qtc2.12015>.
- [14] S. Ecker, B. Liu, J. Handsteiner, M. Fink, D. Rauch, F. Steinlechner, T. Scheidl, A. Zeilinger, and R. Ursin, “Strategies for achieving high key rates in satellite-based QKD,” *npj Quantum Information*, vol. 7, no. 1, p. 5, 2021, <http://doi.org/10.1038/s41534-020-00335-5>.
- [15] V. Acosta, D. Dequal, M. Schiavon, A. Montmerle-Bonnefois, C. Lim, J. Conan, and E. Diamanti, “Analysis of satellite-to-ground quantum key distribution with adaptive optics,” *New Journal of Physics*, vol. 26, no. 2, p. 023039, 2024, <http://doi.org/10.1088/1367-2630/ad231c>.
- [16] L. Ji, J. Gao, A. Yang, Z. Feng, X. Lin, Z. Li, and X. Jin, “Towards quantum communications in free-space seawater,” *Optics Express*, vol. 25, no. 17, pp. 19 795–19 806, 2017, <http://doi.org/10.1364/OE.25.019795>.
- [17] S. Zhao, X. Han, Y. Xiao, Y. Shen, Y. Gu, and W. Li, “Performance of underwater quantum key distribution with polarization encoding in ocean water,” *Journal of the Optical Society of America A*, vol. 36, no. 5, pp. 883–892, 2019, <http://doi.org/10.1364/JOSAA.36.000883>.
- [18] C. H. Bennett and G. Brassard, “Quantum cryptography: Public key distribution and coin tossing,” in *International conference on computers, systems and signal processing*, 1984, pp. 175–179, <http://doi.org/10.1016/j.tcs.2014.05.025>.
- [19] P. W. Shor and J. Preskill, “Simple proof of security of the BB84 quantum key distribution protocol,” *Physical review letters*, vol. 85, no. 20, p. 441, 2000, <http://doi.org/10.1103/PhysRevLett.85.441>.
- [20] Muskan, R. Meena, and S. Banerjee, “Performance analysis of satellite-based QKD protocols using the circular beam model,” *arXiv*, 2023, <https://arxiv.org/abs/2308.01036>.
- [21] Y. Ata and K. Kiasaleh, “Impact of natural turbulent waters on quantum key distribution: Temperature and salinity considerations,” *IEEE Journal of Oceanic Engineering*, vol. 50, no. 3, pp. 2381–2393, 2025, <http://doi.org/10.1109/JOE.2025.3551076>.

- [22] P. Paglierani, A. H. F. Raouf, K. Pelekanakis, R. Petrocchia, J. Alves, and M. Uysal, “A primer on underwater quantum key distribution,” *Quantum Engineering*, vol. 2023, no. 1, p. 7185329, 2023, <http://doi.org/10.1155/2023/7185329>.
- [23] X. B. Wang, “Beating the photon-number-splitting attack in practical quantum cryptography,” *Physical review letters*, vol. 94, no. 23, p. 230503, 2005, <http://doi.org/10.1103/PhysRevLett.94.230503>.
- [24] A. Kumar and S. Garhwal, “State-of-the-art survey of quantum cryptography,” *Archives of Computational Methods in Engineering*, vol. 29, no. 4, pp. 2291–2313, 2021, <http://doi.org/10.1007/s11831-021-09561-2>.
- [25] V. Scarani, H. Bechmann-Pasquinucci, N. J. Cerf, M. Dušek, N. Lütkenhaus, and M. Peev, “Quantum cryptography protocols robust against photon number splitting attacks for weak laser pulse implementations,” *Physical review letters*, vol. 92, no. 5, p. 057901, 2004, <http://doi.org/10.1103/PhysRevLett.92.057901>.
- [26] N. Rizk, A. Drémeau, and A. Coatanhay, “Performances des protocoles QKD, BB84 et SARG04 pour les communications quantiques sous-marines,” in *Proc. of GRETSI, Strasbourg, France, 2025*.
- [27] C. H. Bennett, G. Brassard, and N. D. Mermin, “Quantum cryptography without bell’s theorem,” *Physical review letters*, vol. 68, no. 5, p. 557, 1992, <http://doi.org/10.1103/PhysRevLett.68.557>.
- [28] C. Fung, K. Tamaki, and H. Lo, “On the performance of two protocols: SARG04 and BB84,” *arXiv [quant-ph]*, 2005, <https://arxiv.org/abs/quant-ph/0510025>.
- [29] C. Branciard, N. Gisin, B. Kraus, and V. Scarani, “Security of two quantum cryptography protocols using the same four qubit states,” *Physical Review A*, vol. 72, no. 3, p. 032301, 2005, <http://doi.org/10.1103/PhysRevA.72.032301>.
- [30] E. Waks, H. Krovi, and Y. Yamamoto, “Security of quantum key distribution with entangled photons against individual attacks,” *Physical Review A*, vol. 65, no. 5, p. 052310, 2002, <http://doi.org/10.1103/PhysRevA.65.052310>.
- [31] C. Fung, K. Tamaki, and H. Lo, “Performance of two quantum-key-distribution protocols,” *Physical Review A*, vol. 73, no. 1, p. 012337, 2006, <http://doi.org/10.1103/PhysRevA.73.012337>.
- [32] C. D. Mobley, *Light and water: radiative transfer in natural waters*. Academic press, 1994, ISBN: 978-0-12-502890-7.
- [33] M. Elamassie, F. Miramirkhani, and M. Uysal, “Performance characterization of underwater visible light communication,” *IEEE Transactions on Communications*, vol. 67, no. 1, pp. 543–552, 2018, <http://doi.org/10.1109/TCOMM.2018.2867498>.
- [34] B. Saleh and M. Teich, *Fundamentals of Photonics*. Wiley, 1991, <http://doi.org/10.1002/0471213748>.
- [35] D. Rogers, J. Bienfang, A. Mink, B. Hershman, A. Nakassis, X. Tang, L. Ma, D. Su, C. Williams, and C. Clark, “Free-space quantum cryptography in the H-alpha fraunhofer window,” in *Free-Space Laser Communications VI*, vol. 6304. SPIE, 2006, pp. 296–305, <http://doi.org/10.1117/12.680899>.
- [36] X. Ma, B. Qi, Y. Zhao, and H. Lo, “Practical decoy state for quantum key distribution,” *Physical Review A*, vol. 72, no. 1, p. 012326, 2005, <http://doi.org/10.1103/PhysRevA.72.012326>.
- [37] S. Ali, S. Mohammed, M. Chowdhury, and A. Hasan, “Practical SARG04 quantum key distribution,” *Optical and Quantum Electronics*, vol. 44, no. 10, pp. 471–482, 2012, <http://doi.org/10.1007/s11082-012-9571-2>.
- [38] A. S. Holevo, *Quantum systems, channels, information: a mathematical introduction*. Walter de Gruyter GmbH & Co KG, 2013, <http://doi.org/10.1515/9783110273403>.
- [39] M. Wilde, *Quantum information theory*. Cambridge university press, 2013, <http://doi.org/10.1017/CBO9781139525343>.
- [40] A. de Oliveira, R. Gomes, V. Brasil, N. da Silva, L. Céleri, and P. Ribeiro, “Full thermalization of a photonic qubit,” *Physics Letters A*, vol. 384, no. 36, p. 126933, 2020, <http://doi.org/10.1016/j.physleta.2020.126933>.

- [41] B. Woźniak and J. Dera, *Light Absorption in Sea Water*, ser. Atmospheric and Oceanographic Sciences Library. Springer, 2007, vol. 33, <http://doi.org/10.1007/978-0-387-49560-6>.
- [42] A. H. F. Raouf, “Performance analysis of underwater quantum key distribution in oceanic turbulence channels,” 2022, master’s Thesis.
- [43] H. Singh, D. Gupta, and A. Singh, “Quantum key distribution protocols: a review,” *Journal of Computer Engineering*, vol. 16, no. 2, pp. 1–9, 2014, <http://doi.org/10.9790/0661-162110109>.

Nour Rizk received the M.Sc. degree in Applied Mathematics and Modeling from the Université de Rouen Normandie - UFR Sciences et Techniques, Rouen, France, in 2023. Since 2023, she has been pursuing the Ph.D. degree with the École Nationale Supérieure de Techniques Avancées (ENSTA, Institut Polytechnique de Paris), Brest, France, and the Lab-STICC, CNRS UMR 6285. Her research focuses on quantum optical systems for underwater communication, quantum key distribution, and quantum information theory.

Angélique Drémeau graduated from the IMT Atlantique (ex-ENSTB), Brest, France, in 2006. She received the Ph.D. degree from the University of Rennes, France, in 2010, and the HDR degree from the Université de Bretagne Occidentale (UBO), Brest, France, in December 2022. She is currently a Full Professor at the École Nationale Supérieure de Techniques Avancées (ENSTA, Institut Polytechnique de Paris), Brest. Her research interests include the information theory and wave propagation in complex environments.

Arnaud Coatanhay graduated from the École Supérieure d'Ingénieurs en Génie Electrique (ESIGELEC), Rouen, France, in 1993. He received the Ph.D. degree from the University of Le Havre, Le Havre, France, in 2000, and the HDR degree from the Université de Bretagne Occidentale (UBO), Brest, France, in June 2022. He is currently a Full Professor at the École Nationale Supérieure de Techniques Avancées (ENSTA, Institut Polytechnique de Paris), Brest. His research interests include the modeling of electromagnetic wave propagation in complex and random media. For almost ten years, his research has been devoted more specifically to quantum optics in natural environments, with applications in telecommunications and remote sensing.